Tulips University of Tsukuba Repository

Operation of BaSi2 homojunction solar cells on p+-Si(111) substrates and the effect of structure parameters on their performance

著者（英）	Komomo Kodama, Yudai Yamashita, Kaoru TOKO, Takashi SUEMASU
journal or publication title	Applied physics express
volume	12
number	4
page range	041005
year	2019-04
権利	(C) 2019 The Japan Society of Applied Physics
URL	http://hdl.handle.net/2241/00155620

doi: 10.7567/1882-0786/ab0c4f

Operation of $BaSi_2$ homojunction solar cells on p^+-Si(111) substrates and the effect of structure parameters on their performance

Komomo Kodama[a], Yudai Yamashita[a], Kaoru Toko[a], and Takashi Suemasu[a*]

[a]*Institute of Applied Physics, Graduate School of Pure and Applied Sciences, University of Tsukuba, Tsukuba, Ibaraki 305-8573, Japan*

Operation of n^+-$BaSi_2$/p-$BaSi_2$(500 nm)/p^+-$BaSi_2$ homojunction solar cells on p^+-Si(111) is demonstrated, showing a saturation current density of 9.4 mA/cm^2 and an open-circuit voltage of 0.11 V under AM1.5 illumination. Photogenerated electrons deep in the p-$BaSi_2$ light absorber layer are likely to be transferred to the p^+-Si side, leading to negative values of internal quantum efficiency (*IQE*) at longer wavelengths. The negative *IQE* can be solved by extending the width of depletion region in the p-$BaSi_2$ light absorber layer by decreasing its hole concentration. The importance of Si substrate surface morphology is also discussed.

* Corresponding author at:

Institute of Applied Physics, Faculty of Pure and Applied Sciences, University of Tsukuba, Tsukuba, Ibaraki 305-8573, Japan

Electronic mail: suemasu@bk.tsukuba.ac.jp

26 At present, 90% of the solar cells in the market are based on crystalline silicon (c-Si), and the
27 conversion efficiency (η) of c-Si solar cells has exceeded 26%.[1] η is now approaching the
28 theoretical Shockley-Queisser limit,[2] determined by a narrow bandgap of 1.1 eV. Therefore,
29 alternative wider-bandgap materials such as III-V semiconductors, chalcopyrites, CdTe, and
30 perovskites are being examined.[3-7] Under such circumstances, we have paid special attention to
31 barium disilicide ($BaSi_2$).[8-10] It is composed of earth-abundant Ba and Si, and has attractive
32 features such as a suitable bandgap of 1.3 eV, a large absorption coefficient (α) of 3×10^4 cm$^-$
33 ^{1} at 1.5 eV,[11-14] and a large bulk minority-carrier lifetime of 14 μs.[15] Furthermore, $BaSi_2$
34 epitaxial films can be grown on Si substrates,[16,17] and its bandgap can be increased by adding
35 isoelectric elements like Sr and C.[18,19] $BaSi_2$ is therefore a material of choice for targeting η
36 beyond 30% in a Si-based tandem solar cell. As a first step, we have achieved η approaching
37 10% in B-doped p-$BaSi_2$/n-Si heterojunction solar cells.[20-22] In a p-$BaSi_2$/n-Si solar cell, the
38 built-in potential is as small as 0.2 V due to the low electron affinity of $BaSi_2$ (3.2 eV).[23] The
39 experimentally obtained open-circuit voltage (V_{OC}) was therefore smaller than 0.5 V.[20-22] Hence,
40 it is not easy to make a drastic improvement in the η of p-$BaSi_2$/n-Si solar cells. Therefore, we
41 next moved on to $BaSi_2$ homojunction solar cells, and very recently demonstrated the
42 photogenerated carrier separation by the built-in electric field in these diodes on p^+-Si(111).[24]
43 However, we face two problems, that is, a small saturation current density (J_{SC}) of 1.3 mA/cm^2,
44 and large leakage current.[24] Such a small J_{SC} was caused by zero or even negative internal
45 quantum efficiency (*IQE*) at longer wavelengths around 800–1000 nm. Long wavelength light
46 is absorbed in the deep region of the $BaSi_2$ light absorber layer. Thus, we need to improve the
47 collection of these photogenerated carriers. The large leakage current was caused by defects
48 around the p^+-$BaSi_2$/p^+-Si heterointerface.[25] A p^+-$BaSi_2$/p^+-Si junction is necessary to transfer
49 holes into a p-Si substrate because there is a large valence-band offset (0.65 eV) at the
50 heterointerface.[23] Prior to the growth of $BaSi_2$ layers by molecular beam epitaxy (MBE), the

51 protective oxide layer on the surface has to be removed by heating the substrate at 900 °C for
52 30 min in an ultrahigh-vacuum chamber. This process is called thermal cleaning (TC). Upon
53 this TC, step bunching occurs to a far greater extent especially in the case of a low-resistivity
54 (ρ) Si(111) substrate.[25] Step bunching causes the generation of defects around the p^+-$BaSi_2$/p^+-
55 Si heterointerface, and thus degrades the pn junction, leading to the decrease in shunt resistance
56 R_{SH} as discussed later. We therefore need to prevent this problem, too.

57 In this article, we aim to find solutions to the above two problems, and therefore put
58 emphasis on the following points. First, we extended the depletion region width in a p-$BaSi_2$
59 light absorber layer so that it would be almost fully depleted. This is to efficiently collect the
60 carriers photogenerated in the deep region of the p-$BaSi_2$ absorber layer by the built-in electric
61 field. Second, we employed medium-doped p-Si(111) substrates (ρ = 1–4 Ωcm) rather than p^+-
62 Si(111) substrates to prevent the step bunching upon heating the Si substrates for removing
63 oxides. Heavily p^+-Si layers for a p^+-$BaSi_2$/p^+-Si junction were formed on the surface by
64 implantation of B atoms. As a result, we succeeded to extend the long-wavelength edge of the
65 *IQE* spectrum from 800 to 950 nm, corresponding to the band gap of $BaSi_2$, and achieved the
66 first demonstration of distinct η in a $BaSi_2$ homojunction solar cell. The V_{OC} of 0.11 V, J_{SC} =
67 9.4 mA/cm^2, and η = 0.28% was obtained.

68 We used an ion-pumped MBE system equipped with an electron-beam evaporation
69 source for 10N-Si as well as standard Knudsen cells for 3N-B, 5N-Sb, and 3N-Ba. Details of
70 the growth procedure of undoped $BaSi_2$, Sb-doped n-$BaSi_2$, and B-doped p-$BaSi_2$ layers were
71 reported previously.[20,26,27] Sample structures are summarized in Table I. We used low-ρ n^+-
72 Si(111) substrates (ρ < 0.01 Ωcm) for sample A and p^+-Si(111) substrates (ρ < 0.01 Ωcm) for
73 samples B-E. For sample F, B atoms were implanted into medium-doped p-Si(111) substrates
74 (ρ = 1–4 Ωcm) with a dose of 2.5×10^{14} cm^{-2} and a projected range of 50 nm so that the hole
75 concentration (p) would be approximately 2×10^{19} cm^{-3} on the surface after activation annealing

76 at 900 °C for 3 min. Sample G is a reference to compare the solar cell performance. Samples
77 A-F were fabricated for the following reasons. We formed sample A to confirm the long-
78 wavelength edge where the photoresponsivity sharply arises. For this purpose, we formed a 500
79 nm-thick undoped $BaSi_2$ epitaxial layer by MBE. Then, a 3 nm-thick amorphous Si (a-Si)
80 capping layer was deposited *in situ* at 180 °C to prevent surface oxidation.[28] Finally, 80 nm-
81 thick indium-tin-oxide (ITO) electrode with 1 mm diameter was sputtered on the front side and
82 150-nm-thick Al electrode was sputtered on the back side. In all the samples, a-Si capping
83 layers and electrodes were formed under the same condition as sample A. In samples B-D, we
84 formed three types of $BaSi_2$-pn homojunction diodes, n^+-$BaSi_2$(20 or 150 nm)/p-$BaSi_2$(500
85 nm)/p^+-$BaSi_2$(20 or 50 nm) on p^+-Si(111) substrate ($\rho < 0.01$ Ωcm) to compare their *IQE* spectra.
86 The p of a 500 nm-thick B-doped p-$BaSi_2$ absorber layer was set at approximately 10^{17} cm^{-3}. In
87 samples B and C, we investigated the effect of p^+-$BaSi_2$ layer thickness on the solar cell
88 performance. This is because p^+-$BaSi_2$ layers often degrade the crystalline quality of p-$BaSi_2$
89 light absorber layers. In this respect, p^+-$BaSi_2$ should be as thin as possible. On the other hand,
90 it was reported that p^+-$BaSi_2$ with a certain thickness is necessary to fully cover the p^+-Si
91 substrate.[22] In sample D, the n^+-$BaSi_2$ layer was set at 150 nm so that photons with long
92 wavelengths around 800 nm would be fully absorbed in the p-$BaSi_2$ light absorber layer. In
93 samples E and F, we employed undoped p-$BaSi_2$ layers with p~10^{16} cm^{-3} instead of B-doped p-
94 $BaSi_2$ layers,[29] and investigated the effect of depletion region width in the $BaSi_2$ light absorber
95 layer as well as of the substrate surface morphology on the *IQE* spectra.

96 The current density versus voltage (*J*-*V*) characteristics under standard AM 1.5
97 illumination and photoresponse properties were measured. The photoresponse spectrum was
98 measured using a xenon lamp with a 25-cm-focal-length single monochromator (Bunko Keiki
99 SM-1700A and RU-60N). Reflectance spectra were evaluated with a reflection measurement
100 system using a xenon lamp with an integrating sphere. All measurements were performed at

101 room temperature. The band alignments of samples C and E were simulated by automat for
102 simulation of heterostructures (AFORS-HET), where the ideal condition such as no defects was
103 assumed.[30]

104

105 Table I. Sample preparation details. Si substrate, thicknesses and designed carrier
106 concentrations of p^+- $BaSi_2$, p-$BaSi_2$ light absorber, and n^+-$BaSi_2$ are given.

Sample	Si substrate	p^+-$BaSi_2$	p-$BaSi_2$ absorber	n^+-$BaSi_2$
A	n^+-Si(111), $\rho < 0.01$ Ωcm	–	Undoped, 500 nm $p \sim 10^{15}$ cm^{-3}	–
B	p^+-Si(111), $\rho < 0.01$ Ωcm	B-doped, 50 nm, $p \sim 10^{19}$ cm^{-3}	B-doped, 500 nm, $p \sim 10^{17}$ cm^{-3}	Sb-doped, 20 nm, $n \sim 10^{19}$ cm^{-3}
C	p^+-Si(111), $\rho < 0.01$ Ωcm	B-doped, 20 nm, $p \sim 10^{19}$ cm^{-3}	B-doped, 500 nm, $p \sim 10^{17}$ cm^{-3}	Sb-doped, 20 nm, $n \sim 10^{19}$ cm^{-3}
D	p^+-Si(111), $\rho < 0.01$ Ωcm	B-doped, 20 nm, $p \sim 10^{19}$ cm^{-3}	B-doped, 500 nm, $p \sim 10^{17}$ cm^{-3}	Sb-doped, 150 nm, $n \sim 10^{19}$ cm^{-3}
E	p^+-Si(111), $\rho < 0.01$ Ωcm	B-doped, 20 nm, $p \sim 10^{19}$ cm^{-3}	Undoped, 500 nm, $p \sim 10^{16}$ cm^{-3}	Sb-doped, 20 nm, $n \sim 10^{19}$ cm^{-3}
F	implanted p^+-Si/ p-Si(111), $\rho = 1$–4 Ωcm	B-doped, 20 nm, $p \sim 10^{19}$ cm^{-3}	Undoped, 500 nm, $p \sim 10^{16}$ cm^{-3}	Sb-doped, 20 nm, $n \sim 10^{19}$ cm^{-3}
G[21]	n-Si(111), $\rho = 1$–4 Ωcm	B-doped, 20 nm, $p \sim 10^{18}$ cm^{-3}	–	–

107

108 Figure 1(a) shows the photoresponse spectrum of sample A. A bias voltage (V_{bias}) of 1
109 V was applied to the front ITO electrode with respect to the back Al electrode to collect

110 photogenerated electrons to the ITO. V_{bias} was necessary to extract photogenerated carriers for
111 sample A because there was no built-in electric field in sample A. The photoresponsivity
112 appeared pronounced at wavelengths shorter than approximately 1000 nm, close to the band
113 gap of $BaSi_2$. Figure 1(b) shows the *IQE* spectra of samples B–E for $BaSi_2$ homojunction solar
114 cells, obtained at V_{bias} = 0 V, showing that the built-in electric field surely separated
115 photogenerated carriers. Compared with the spectrum of sample A in Fig. 1(a), however, the
116 *IQE* values at wavelengths between 800 and 1000 nm were negligibly small or even negative
117 in samples B–D. This trend was pronounced in sample D. These results show that the
118 photogenerated carriers deep in the p-$BaSi_2$ absorber layer are difficult to be extracted by the
119 built-in electric field or are transferred in the opposite direction. Figure 1(c) shows the V_{bias}
120 dependences of *IQE* spectra for sample D. With increasing V_{bias} from 0 to 0.2 V to extract
121 photogenerated electrons to the ITO electrode, the *IQE* becomes positive in the whole
122 wavelength region. In sample D, the total thickness of n^+-$BaSi_2$ and p-$BaSi_2$ layers is 650 nm.
123 The value of α at a wavelength of 800 nm is around 3×10^4 cm^{-1}, meaning that the penetration
124 depth at this wavelength is estimated to be $2/\alpha$ = 0.66 μm. Therefore, photons with this
125 wavelength are fully absorbed in the 500 nm-thick p-$BaSi_2$ absorber layer. This is the reason
126 why the negative *IQE* was distinct in sample C. We discuss this result by using the band
127 alignment of sample C shown in Fig. 2(a). The bottom of the conduction band (E_C) of the neutral
128 p-$BaSi_2$ region is positioned a little higher than that of p^+-Si. Therefore, the photogenerated
129 electrons in the deep neutral p-$BaSi_2$ region are likely to be transferred to the p-Si side. We
130 think that such flow of carriers is promoted because there is a number of defect levels at the p^+-
131 $BaSi_2$/p^+-Si interface. On the other hand, in sample E, the long-wavelength edge of the *IQE*
132 spectrum shifted from 800 to 850 nm in Fig. 1(b). We ascribed this shift to the decrease of p in
133 the p-$BaSi_2$ absorber layer from approximately 10^{17} to 10^{16} cm^{-3}. Figure 2(b) shows the band
134 alignment of sample E, where the width of depletion region increased by approximately 3 times

135 compared to that in sample C shown in Fig. 2(a). Please note that the absorber layer is almost
136 fully depleted in sample E, and thereby the electric field might promote the separation of
137 photogenerated carriers, resulting in the improved *IQE* in the long wavelength range. The *IQE*
138 spectrum was further improved in sample F.

139 Figure 3(a) shows the *IQE* spectra of samples E and F. In sample F, the long-
140 wavelength edge of the *IQE* spectrum further shifted from 850 to 950 nm, almost close to the
141 band gap of $BaSi_2$. This result shows that the formation of p^+-Si surface layer by implanting B
142 at a position slightly deeper from the surface is an effective means to extend the *IQE* spectrum
143 toward the longer wavelength range. However, the *IQE* was decreased unexpectedly in the short
144 wavelength range when we compared the *IQE* spectra of samples E and F in Fig. 3(a) with those
145 of samples B–D in Fig. 1(a). This means that the collection of photogenerated carriers in the
146 region close to the surface was degraded in samples E and F. The difference between them is
147 that undoped p-$BaSi_2$ layers were adopted in samples E and F, whereas B-doped p-$BaSi_2$ layers
148 were used in samples B–D. We speculate that the carrier type of the undoped $BaSi_2$ absorber
149 layer in samples E and F would change from p-type to n-type in the region somewhere in the
150 $BaSi_2$ light absorber layer, leading to the decrease in built-in electric field there, and thus
151 degrading the *IQE* in the short wavelength range. This is because undoped p-$BaSi_2$ layers
152 change to an n-type conductivity when the Ba to Si atomic ratio deviates from stoichiometry,
153 and the supply of Si atoms from the Si substrate tends to be deficient as moving towards the
154 surface of $BaSi_2$ layers.[26] Therefore, the formation of lightly-B doped p-$BaSi_2$ layers with $p \sim$
155 10^{16} cm^{-3} is mandatory to improve the *IQE* spectrum, and this would be our key challenge.

156 The *J*-*V* curves under AM 1.5 illumination for samples B, E and F are shown in Fig.
157 3(b). V_{OC} and J_{SC} were improved significantly in samples E and F compared to sample B.
158 Sample F showed $\eta = 0.28\%$, $J_{SC} = 9.42$ mA/cm^2, and $V_{OC} = 0.11$ V. To accurately determine
159 the series resistance (R_S) and R_{SH} of a diode, we adopted a technique described by Sites and

160 Mauk,[31] and summarized in Table II.

161 Table II. Solar cell parameters of samples E, F, and G.[21]

Sample	J_{SC} [mA/cm^2]	V_{OC} [V]	R_S [Ω]	R_{SH} [Ω]	η [%]
E	4.3	0.034	149	1430	0.04
F	9.4	0.113	145	6954	0.28
G[21]	35.2	0.476	128	10046	9.9

162

163 R_{SH} differs significantly between samples E-G, whereas there is not so much difference in R_S.
164 In sample E, the R_{SH} is the smallest, meaning that the leakage current is the highest. The R_{SH}
165 increases in the order of samples E, F, and G. We attribute a small R_{SH} to defects around the p$^+$-
166 $BaSi_2$/p$^+$-Si interface because surface morphology of a Si substrate before the growth of $BaSi_2$
167 layers affects the formation of defects significantly.[25] Figure 4 shows the atomic force
168 microscopy (AFM) topographic views (2 × 2 μm^2) and cross-sectional profiles (along while
169 lines) of the Si substrate surfaces of these samples taken after TC. The root-mean-square (RMS)
170 surface roughness values and reflection high-energy electron diffraction (RHEED) patterns are
171 also presented. The minimum step height of the Si(111) surface is 0.31 nm, and such a surface
172 was obtained in Fig. 4(c) for sample G. The RHEED pattern was surely on the Laue ring,
173 meaning the atomically flat surface. Similar RHEED pattern was obtained in Fig. 4(b) for
174 sample F. On the other hand, in Fig. 4(a), streaky RHEED pattern was observed for sample E,
175 showing the degradation of surface smoothness compared to sample F. Furthermore, the step
176 edge on the surface was not straight but rather complex. We speculate that this kind of
177 difference in surface morphology of the p$^+$-Si(111) surface prior to the growth of $BaSi_2$ films
178 affects the defect formation around the p$^+$-$BaSi_2$/p$^+$-Si interface. Therefore, realization of a
179 smooth p$^+$-Si(111) surface while ensuring a good electrical contact between p$^+$-$BaSi_2$/p$^+$-Si is

180 the key to increasing R_{SH}, and thereby achieving higher η.

181 In summary, we formed several kinds of $BaSi_2$ homojunction solar cells with a 500
182 nm-thick p-$BaSi_2$ light absorber layer. When the hole concentration of the p-$BaSi_2$ absorber
183 layer was approximately 10^{17} cm^{-3}, the *IQE* was almost zero or negative at long wavelengths.
184 This problem was improved drastically by decreasing the p down to 10^{16} cm^{-3}, and by using B
185 implanted medium-doped p-Si(111) substrate. The long-wavelength edge of the *IQE* spectrum
186 extended to around 950 nm, leading to the first demonstration of $BaSi_2$ solar cells with distinct
187 η = 0.28%, V_{OC} = 0.11 V, and J_{SC} = 9.4 mA/cm^2.

188

189 **Acknowledgements**

190 This work was financially supported by JSPS KAKENHI Grant Numbers 17K18865 and
191 18H03767 and JST MIRAI.

192

193 **References**

194 [1] K. Yoshikawa, H. Kawasaki, W. Yoshida, K. Konishi, K. Nakao, T. Uto, D. Adachi, M.
195 Kanematsu, H. Uzu, and K. Yamamoto, Nat. Energy **2**, 17032 (2017).
196 [2] W. Shockley, and H. J. Queisser, J. Appl. Phys. **32**, 510 (1961).
197 [3] P. Jackson, D. Hariskos, R. Wuerz, O. Kiowski, A. Bauer, T. M. Friedlmeier, and M.
198 Powalla, Phys. Status Solidi RRL **9**, 28 (2015).
199 [4] P. Jackson, R. Wuerz, D. Hariskos, E. Lotter, W. Witte, and M. Powalla, Phys. Status Solidi
200 RRL **10**, 583 (2016).
201 [5] X. Wu, Sol. Energy **77**, 803 (2004).
202 [6] J. Burschka, N. Pellet, Soo-Jin Moon, R. Humphry-Baker, P. Gao, M. K. Nazeeruddin, and
203 M. Grätzel, Nature **499**, 316 (2013).
204 [7] W. S. Yang, J. H. Noh, N. J. Jeon, Y. C. Kim, S. Ryu, J. Seo, and S. I. Seok, Science **348**,
205 1234 (2015).
206 [8] T. Nakamura, T. Suemasu, K. Takakura, F. Hasegawa, A. Wakahara, and M. Imai, Appl.
207 Phys. Lett. 81, 1032 (2002).
208 [9] T. Suemasu, Jpn. J. Appl. Phys., Part 1 **54**, 07JA01 (2015).
209 [10] T. Suemasu and N. Usami, J. Phys. D: Appl. Phys. **50**, 023001 (2017).
210 [11] K. Morita, Y. Inomata, and T. Suemasu, Thin Solid Films **508**, 363 (2006)
211 [12] D. B. Migas, V. L. Shaposhnikov, and V. E. Borisenko, Phys. Status Solidi (b) **244**, 2611
212 (2007).
213 [13] K. Toh, T. Saito, and T. Suemasu, Jpn. J. Appl. Phys. **50**, 068001 (2011).
214 [14] M. Kumar, N. Umezawa, and M. Imai, Appl. Phys. Express **7**, 071203 (2014).
215 [15] K. O. Hara, N. Usami, K. Nakamura, R. Takabe, M. Baba, K. Toko, and T. Suemasu, Appl.
216 Phys. Express **6**, 112302 (2013).
217 [16] R. A. McKee, F. J. Walker, J. R. Conner, E. D. Specht, and D. E. Zelmon, Appl. Phys.
218 Lett. 59, 782 (1991).
219 [17] R. A. McKee and F. J. Walker, Appl. Phys. Lett. 63, 2818 (1993).
220 [18] K. Morita, M. Kobayashi, and T. Suemasu, Jpn. J. Appl. Phys. **45**, L390 (2006).
221 [19] Y. Imai and A. Watanabe, Intermetallics **18**, 1432 (2010).
222 [20] D. Tsukahara, S. Yachi, H. Takeuchi, R. Takabe, W. Du, M. Baba, Y. Li, K. Toko, N.
223 Usami, and T. Suemasu, Appl. Phys. Lett. **108**, 152101 (2016).
224 [21] S. Yachi, R. Takabe, H. Takeuchi, K. Toko, and T. Suemasu, Appl. Phys. Lett. **109**, 072103
225 (2016).

226 [22] T. Deng, T. Sato, Z. Xu, R. Takabe, S. Yachi, Y. Yamashita, K. Toko, and T. Suemasu,
227 Appl. Phys. Express **11**, 062301 (2018).
228 [23] T. Suemasu, K. Morita, M. Kobayashi, M. Saida, and M. Sasaki, Jpn. J. Appl. Phys. **45**,
229 L519 (2006).
230 [24] K. Kodama, R. Takabe, T. Deng, K. Toko, and T. Suemasu, Jpn. J. Appl. Phys. **57**, 050310
231 (2018).
232 [25] Y. Yamashita, S. Yachi, R. Takabe, T. Sato, M. Emha Bayu, K. Toko, and T. Suemasu,
233 Jpn. J. Appl. Phys. **57**, 025501 (2018).
234 [26] R. Takabe, T. Deng, K. Komomo, Y. Yamashita, T. Sato, K. Toko, and T. Suemasu, J.
235 Appl. Phys. **23**, 045703 (2018).
236 [27] K. Kodama, R. Takabe, S. Yachi, K. Toko, and T. suemasu, Jpn. J. Appl. Phys. **57**, 031202
237 (2018).
238 [28] R. Takabe, H, Takeuchi, W. Du, K. Ito, K. Toko, S. Ueda, A. Kimura, and T. Suemasu, J.
239 Appl. Phys. **119**, 165304 (2016).
240 [29] Y. Yamashita, T. Sato, K. Toko, A. Uedono, and T. Suemasu, Ext. Abstr. (79th Autumn
241 Meet., 2018), Japan Society of Applied Physics and Related Societies, 19p-436-15 [in
242 Japanese].
243 [30] R. Varache, C. Leendertz, M. E. Gueunier-Farret, J. Haschke, D. Muñoz, and L. Korte,
244 Sol. Energy Mater. Sol. Cells **141**, 14 (2015).
245 [31] J. R. Sites and P. H. Mauk, Sol. Cells **27**, 411 (1989).
246
247

248 **Figure captions**

249 Fig. 1. (a) Photoresponse spectrum of sample A, 500 nm-thick undoped $BaSi_2$ layer with R_{Ba}/R_{Si}
250 ~ 2, measured under a bias voltage of 1 V applied to the front ITO electrode with respect to the
251 back Al electrode. (b) *IQE* spectra of samples B−E.

252

253 Fig. 2. Calculated band alignments of $BaSi_2$ n^+-p-p^+ homojunction diodes on p^+-Si(111) by
254 AFORS-HET for (a) sample C and (b) sample E. The p of the p-$BaSi_2$ absorber layer is
255 approximately 10^{17} cm^{-3} in sample C and 10^{16} cm^{-3} in sample E. The arrows indicate the flow
256 of photogenerated electrons.

257

258 Fig. 3. (a) *IQE* spectra of samples E and F and (b) *J*-*V* characteristics of samples B, E, and F
259 under AM1.5 illumination.

260

261 Fig. 4. Topographic AFM views (2×2 μm^2) and cross-sectional profiles (along white lines) of
262 the Si substrate surface taken after the thermal cleaning in UHV for samples (a) E, (b) F and (c)
263 G. RMS surface roughness values and RHEED patterns are presented.

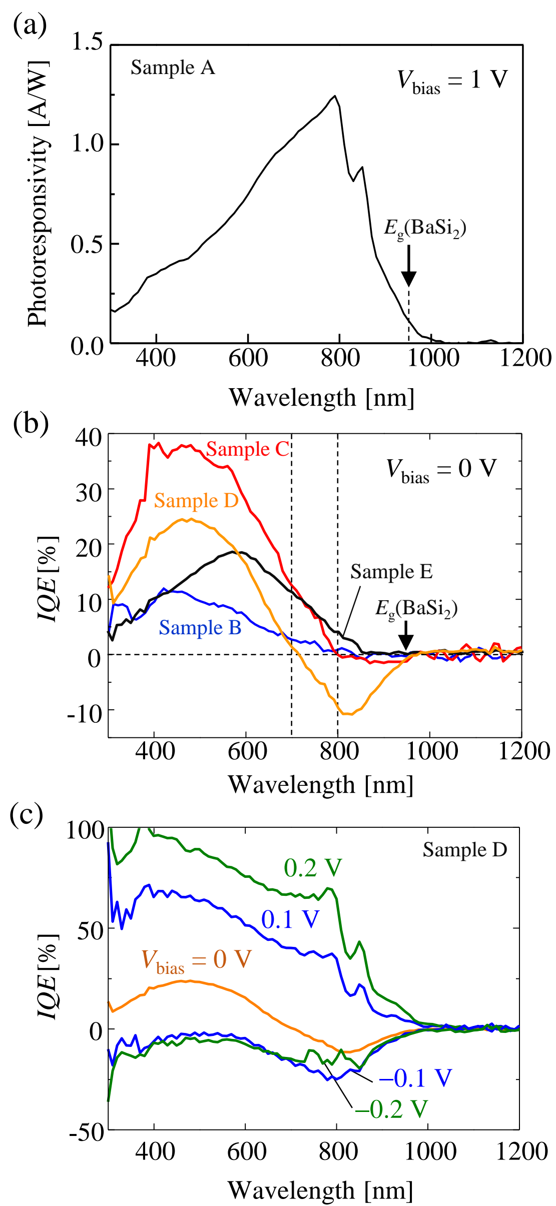

Fig. 1

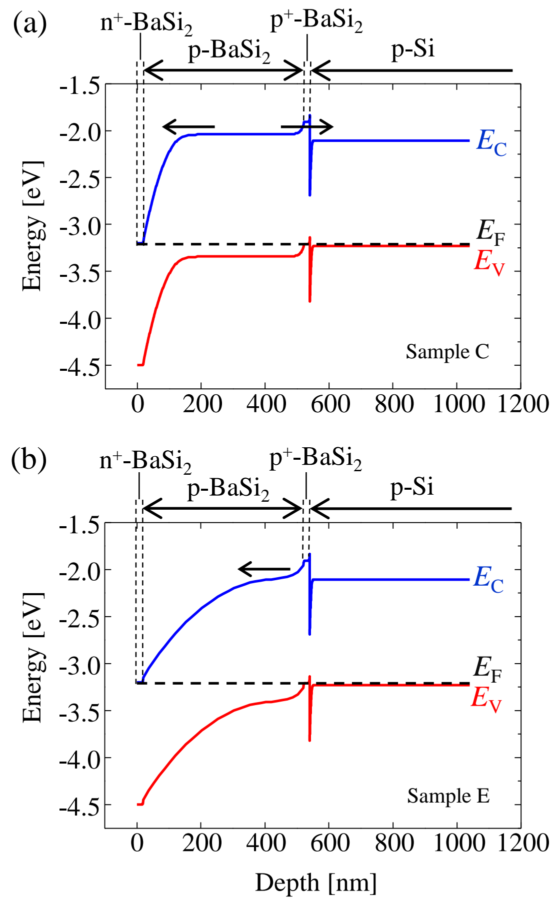

Fig. 2

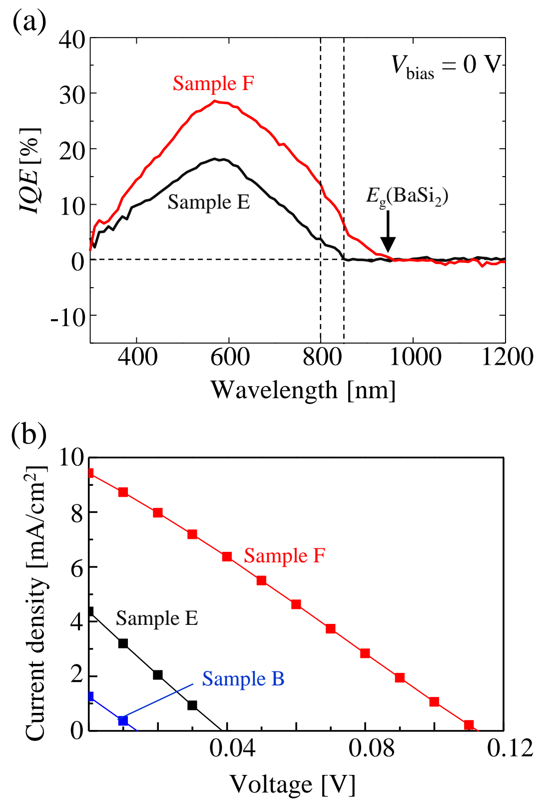

Fig. 3

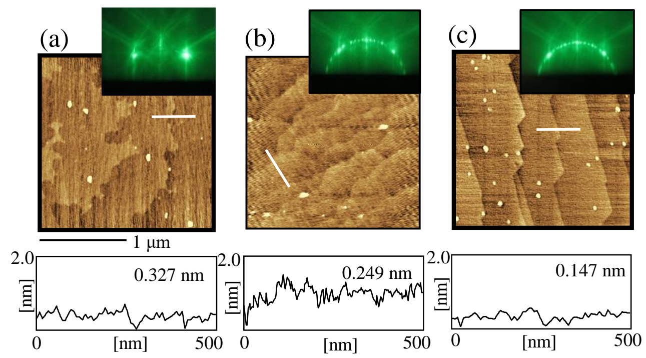

Fig. 4